Supporting Information

Holistic Bulk-to-Surface Tailoring of Ni-Rich Cathodes for Unlocking Superior Electrochemical Stability

Yang Li,[#a] Zhixuan Liu,[#d] Haoji Wang,*[c] Jun Chen,*[c,d] Zebo Gu,[b] Junyong Deng,[b] Guorong Liu,[b] Kun Huang,[b] Siyao Zhang,[b] Hao Feng,[b] Hao Chen,[b] Hongxin He,[a] Fuliang Zhu,[e] Lina Hu,[b] Hongshuai Hou*[c] and Xiaobo Ji*[c]

[a] College of Materials Science and Engineering, Yangtze Normal University, Chongqing 408100, China.

[b] CVC Testing Technology Co., Ltd., China National Electric Apparatus Research Institute Co., Ltd., Guangzhou 510000, China

[c] College of Chemistry and Chemical Engineering, Central South University, Changsha 410083, China

[d] Department of Chemistry/Department of Environment and Geography, University of York, York YO10 5DD, England

[e] School of Metallurgy and Environment, Lanzhou University of Technology, Lanzhou 730050, China

E-mail: wanghaoji_csu@163.com; J-Chen@cei1958.com; hs-hou@csu.edu.cn

Experimental Section/Methods

Material preparation: The NCM83 and NCM83-xBC compounds were fabricated using a solid-phase synthesis approach. The $Ni_{0.83}Co_{0.07}Mn_{0.1}(OH)_2$ precursor employed in the co-precipitation process was commercially sourced from Zhejiang Electric Power New Energy Co., Ltd. In the case of NCM83 production, precisely measured quantities of $Ni_{0.83}Co_{0.07}Mn_{0.1}(OH)_2$ and $LiOH{\cdot}H_2O$ (acquired from Aladdin Reagent, Shanghai) were combined in a 1:1.05 molar ratio, then subjected to ethanol-based ball-milling at 500 rpm for 12 hours. The processed blend was subsequently calcined in an oxygen environment, first at 500 °C for 5 hours, then at 780 °C for 15 hours to yield the final NCM83 material. For creating B/Ce co-doped NCM83 variants (NCM83-xBC), calculated quantities of B_2O_3 and $Ce(NO_3)_4$ were introduced into an ethanol suspension containing NCM83, followed by 2 hours of ball-milling. The resulting mixture underwent heat treatment at 600 °C. Modified specimens with different B/Ce doping levels (1.0, 1.5, and 2.0 atomic percent) were produced, labeled as NCM83-1.0BC, NCM83-1.5BC, and NCM83-2.0BC accordingly. All prepared samples were preserved in an argon atmosphere glove box to avoid hydration.

Materials Characterization: The crystallographic phases and structural properties of the samples were analyzed using X-ray diffraction (XRD, Bruker D8 Advance, Cu Kα radiation) with a scanning angle from 10° to 80° (2θ). GSAS software was utilized for Rietveld refinement of the collected XRD patterns. Field emission scanning electron microscopy (FESEM, Hitachi SU8010) and transmission electron microscopy (JEM-2100F) were employed to investigate the surface morphology and microstructural features. For atomic-scale characterization after electrochemical cycling, a dual-beam system combining focused ion beam (FIB, Thermo Scientific Helios 5 CX) with high-angle annular dark-field scanning transmission electron microscopy (HAADF-STEM, Thermo Scientific Themis Z) was implemented. X-ray absorption fine structure (XAFS) measurements were conducted in transmission mode using a RapidXAFS 2M spectrometer (Anhui Absorption Spectroscopy Analysis Instrument Co., Ltd.) operating at 20 kV and 20 mA, with a spherical bent crystal analyzer (Si (551), 500 mm curvature radius) specifically configured for nickel analysis. Elemental composition was determined by inductively coupled plasma optical emission spectrometry (ICP-OES, PerkinElmer 8300), while X-ray photoelectron spectroscopy (XPS, Thermo Fisher Scientific) was used to examine surface chemical states.

Electrochemical characterization: The NCM83 and NCM83-xBC samples were subjected to electrochemical evaluation using CR-2032 coin cells assembled under an argon atmosphere. Cathode fabrication involved blending the active material with polyvinylidene fluoride binder and conductive carbon (90:5:5 weight ratio) in N-methyl-2-pyrrolidone to form a uniform slurry, which was subsequently applied onto aluminum current collectors and vacuum-dried at 80°C for 12 hours. The resulting cathodes exhibited an areal mass loading of 3-4 mg/cm². The electrochemical cells incorporated lithium metal anodes, Celgard 2400 separators, and 1 M LiPF6 electrolyte solution in EC/DMC (1:1 v/v). Room-temperature galvanostatic cycling was performed using a LAND CT2001A test system (Wuhan, China). Galvanostatic intermittent titration technique (GITT) measurements involved 0.1 C charging pulses (10 min duration) followed by 50 min relaxation periods until reaching 4.5 V cutoff. Electrochemical impedance spectroscopy (0.01 Hz-100 kHz)

and cyclic voltammetry (0.1-0.5 mV/s) were conducted using a CHI 660E potentiostat. In situ XRD characterization was carried out during 0.1 C cycling (2.7-4.5 V) using a specialized beryllium-window cell (Beijing SCAST Technology Co., Ltd.).

DFT calculations: We were conducted using the Vienna Ab Initio Simulation Package (VASP) for density functional theory (DFT) computations. The generalized gradient approximation (GGA) with the Perdew-Burke-Ernzerhof (PBE) functional was adopted. Core electrons were represented by projector augmented wave (PAW) potentials, while valence electrons were treated with a plane-wave basis set having a kinetic energy cutoff of 500 eV. The Gaussian smearing technique (width = 0.05 eV) was applied for partial orbital occupancies. Self-consistency was achieved when successive electronic energy differences fell below 1×10^{-5} eV. Structural relaxation convergence was set at forces below 0.05 eV $Å^{-1}$. Van der Waals interactions were incorporated through Grimme's DFT-D3 correction scheme. Initial optimizations employed gamma-point sampling in reciprocal space, permitting full atomic relaxation. Lithium ion migration pathways were investigated via the nudged elastic band (NEB) approach, which interpolates between initial and final states using discrete intermediate configurations. Defect formation energies were computed as Ef=E(total)-EV(total)-1/2E(O_2), where E(total) denotes the total system's energy, EV(total) represents the pristine structure, and EO2 corresponds to the gaseous oxygen molecule energy.

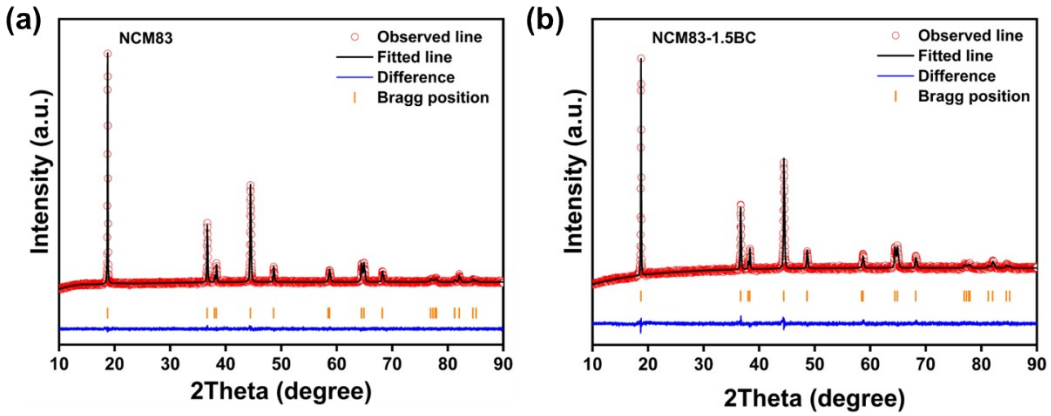

Figure S1. Rietveld refinement of the XRD for the NCM83 and NCM83-1.5BC cathode.

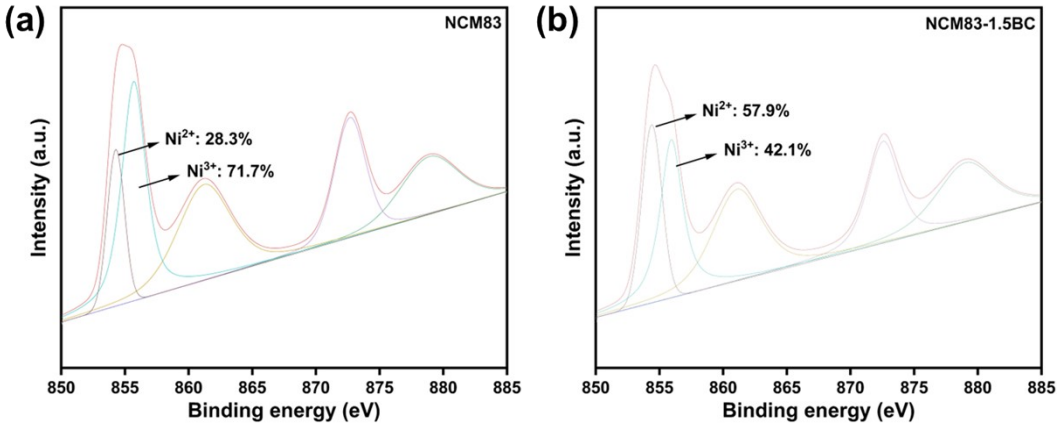

Figure S2. XPS spectra and fitting results of Ni of the NCM83 and NCM83-1.5BC cathode.

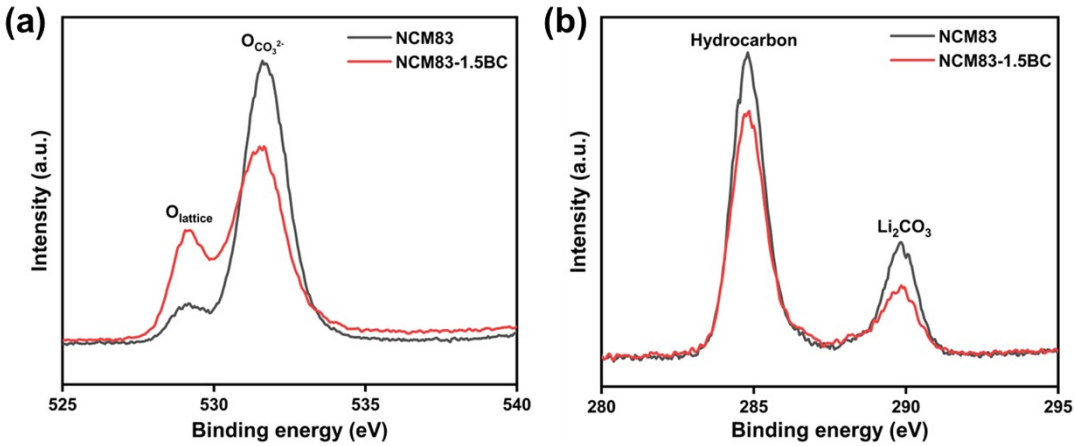

Figure S3. XPS spectra of the NCM83 and NCM83-1.5BC cathode: (a) O 1s, (b) C 1s.

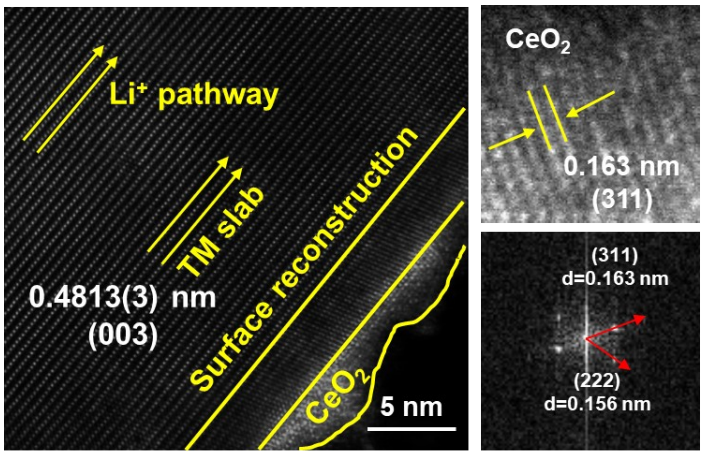

Figure S4. The HAADF-STEM image of the NCM83-1.5BC cathode.

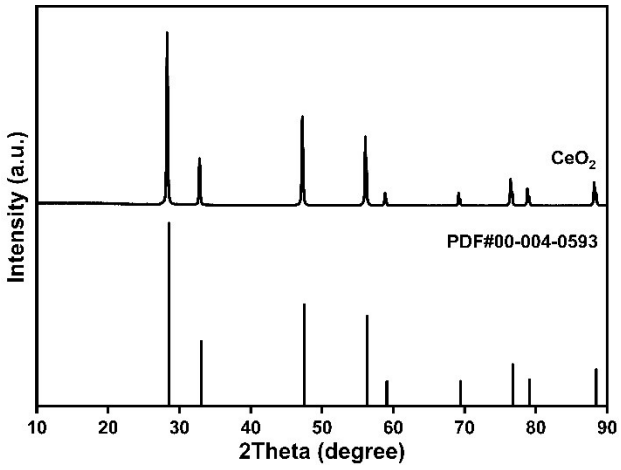

Figure S5. XRD patterns of the obtained CeO_2.

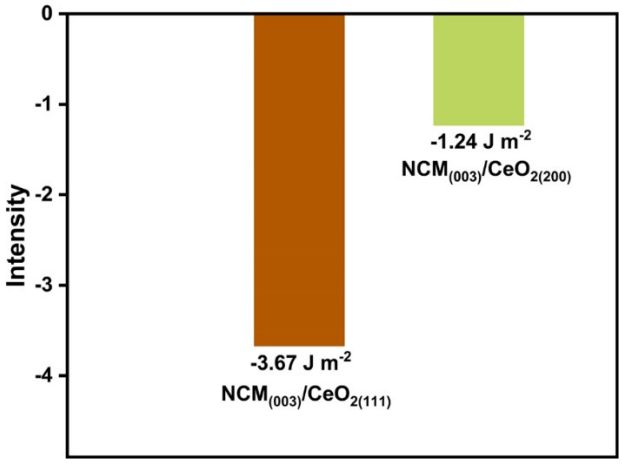

Figure S6. The interface structure of NCM83/CeO_2.

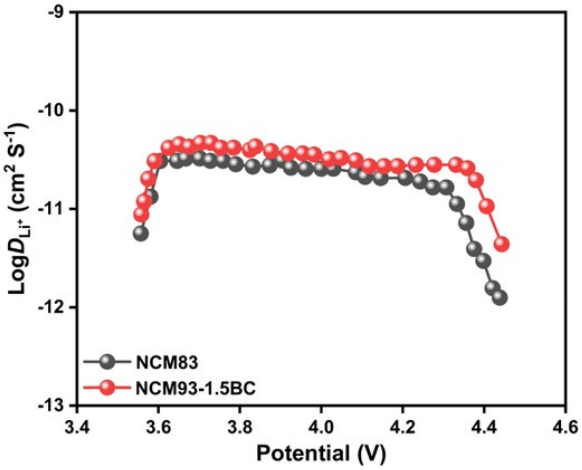

Figure S7. The Li^+ diffusion of the NCM83 and NCM83-1.5BC cathode obtained by the GITT.

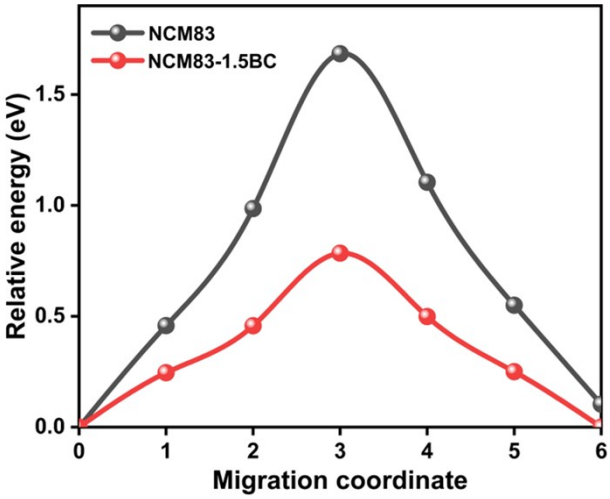

Figure S8. Migration energy barriers in NCM83 and NCM83-1.5BC.

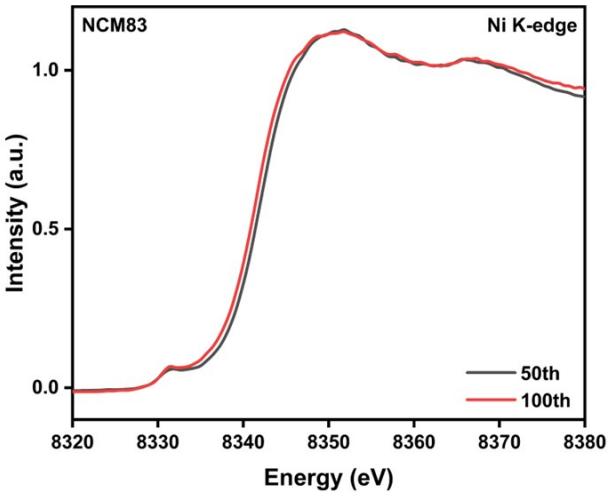

Figure S9. The XANES spectra of NCM83 in the fully delithiated state.

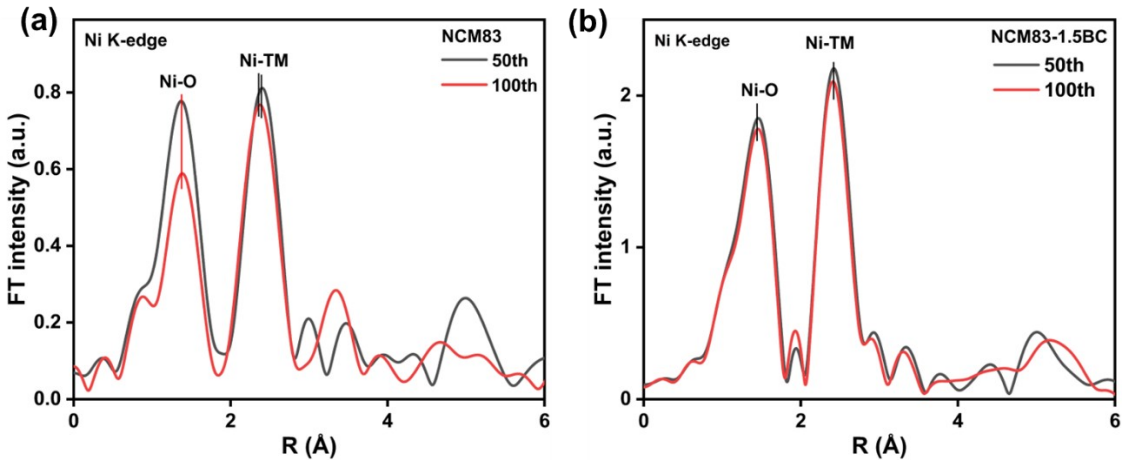

Figure S10. EXAFS of pristine and cycled (a) NCM83 and (b) NCM83-1.5BC in the fully delithiated state.

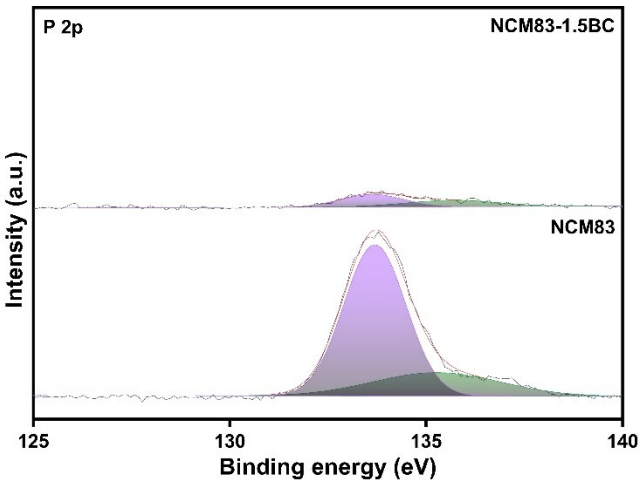

Figure S11. XPS of P 2p for NCM83 and NCM83-1.5BC after 100th cycles between 2.7-4.5 V.

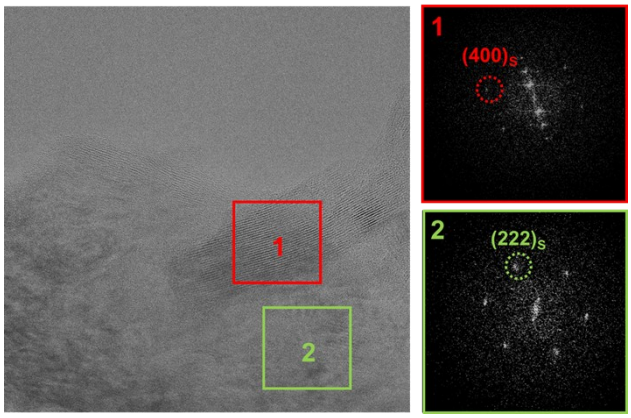

Figure S12. Cryo-EM images of NCM83 cathode surface after 100 cycles.

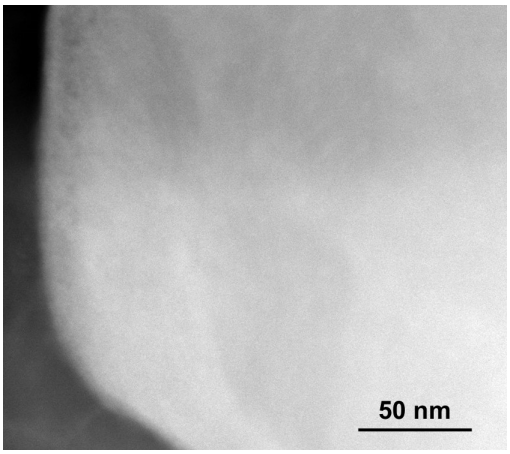

Figure S13. Low-magnification HAADF-STEM images of cross-section for NCM83-1.5BC after 200 cycles at 1 C

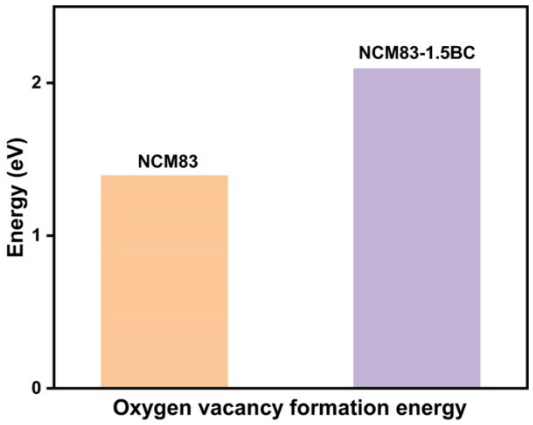

Figure S14. O-vacancy formation energy of NCM83 and NCM83-1.5BC.

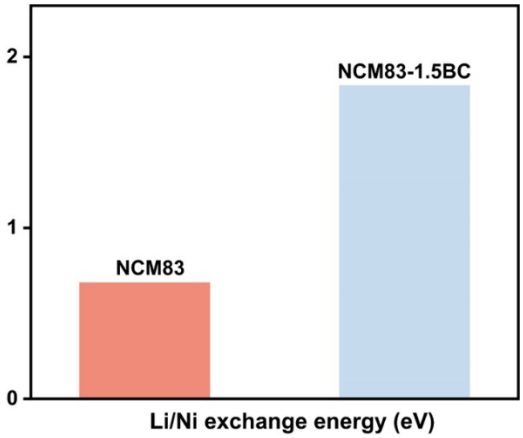

Figure S15. The formation energies of Li^{+}/Ni^{2+} mixing of NCM83 and NCM83-1.5BC.

Table S1. The chemical compositions of Ni, Co, Mn, Ce, and B for NCM83 and NCM83-1.5BC samples based on ICP test.

Sample	Ni (at%)	Co (at%)	Mn (at%)	Ce (at%)	B (at%)
NCM83	83.012	6.99	10.12	/	/
NCM83-1.5BC	82.987	6.93	10.12	1.476	1.489

Table S2. Rietveld-refined XRD results of NCM83 and NCM83-1.5BC cathodes.

Cathode	*a*(Å)	*c*(Å)	*V*(Å^3)	Ni in Li (%)	$I_{(003)}/I_{(104)}$	h_{Li-O}(Å)	h_{TM-O}(Å)
NCM83	2.8613	14.1634	101.17	2.37	1.73	2.1137	2.5837
NCM83-1.5BC	2.8598	14.1913	101.27	2.83	1.69	2.1386	2.5826